PERGAMON

International Journal of Heat and Mass Transfer 45 (2002) 2243–2253

International Journal of HEAT and MASS TRANSFER

www.elsevier.com/locate/ijhmt

Effective thermal conductivity of compressed woods

Yutaka Asako *, Hisayoshi Kamikoga, Hisashi Nishimura, Yoshiyuki Yamaguchi

Department of Mechanical Engineering, Tokyo Metropolitan University, 1-1 Minami-Osawa, Hachioji, Tokyo 192-0397, Japan

Received 4 July 2001; received in revised form 19 October 2001

Abstract

Compression is one solution to improve the strength of softwoods. The effective thermal conductivities of compressed Japanese cedars (*cryptomeria japonica*), which were compressed in the radial direction of the wood, were measured. Both the effective thermal conductivities in the tangential and fiber directions increase proportionally to the density increment due to the compression. However, the thermal conductivity in the radial direction (compression direction) increases slightly with the density increment. Numerical computations were conducted to explain the characteristics of thermal conductivity in the radial direction by using a microscopic heat conduction model for the compressed wood. The numerical results were compared with the measured values. And the physical mechanism of the heat conduction in the compressed woods is discussed.

1. Introduction

The total amount of woods consumed in Japan during a year reaches 1.1 billion cubic meters. However, 75% of them are imported. On the other hand, the resource of 1.1 billion cubic meters grows every year in the domestic forest. Therefore, the resource in the domestic forest accumulates year by year. This is due to the price difference between the domestic and imported woods and most of the resources in the domestic forest is Japanese cedar (*cryptomeria japonica*) being softwood. It is strongly required to improve the quality of domestic wood which is compression of the wood [1]. It results in good strength characteristics.

Aluminum window frames are widely used in Japan. To suppress the energy loss through the window frame, the development of a thermal insulating window frame is strongly required. Generally, the effective thermal conductivity of wood is lower than that of metal. Therefore, the window frame is one of the uses of the compressed wood. A careful search of the literature failed to disclose any prior work on the effective thermal conductivity of compressed woods. This has motivated the present study to measure the thermal conductivity of compressed Japanese cedars.

In this study, the effective thermal conductivities in each direction of the compressed woods, which were compressed in the radial direction, were measured. The measured thermal conductivities in the tangential and fiber directions increase proportionally to the density increment due to the compression. However, the thermal conductivity in the radial direction (compression direction) increases slightly with the density increment. Then, a one-dimensional heat conduction analysis was conducted to explain the characteristics of thermal conductivity of the compressed wood. The characteristics of the thermal conductivity in the tangential and fiber directions were explained by the one-dimensional model but it failed to explain the characteristics of the thermal conductivity in the radial direction. Then, numerical computations were conducted to explain the characteristics of thermal conductivity in the radial direction by using a microscopic heat conduction model for the compressed wood. The numerical results were compared with measured thermal conductivities. And the physical mechanisms of the heat conduction in the compressed woods are discussed.

* Corresponding author. Tel.: +81-426-77-2711; fax: +81-426-77-2701.

E-mail address: asako@ecomp.metro-u.ac.jp (Y. Asako).

0017-9310/02/$ - see front matter
PII: S0017-9310(01)00330-1

Nomenclature

C_r	compression ratio $= \rho_0/\rho$
c	specific heat, J/kg K
D	width of medium, m
d	width of hot-wire, m
H	half height of cell, m
h	height of wood, m
$\dot{q}$	conduction heat flux, W/m^2
$\dot{q}_{wire}$	heat generation in hot-wire, W/m
$\dot{Q}$	heat conduction rate, W
T	temperature, K
t	time, s
u	moisture content, kg-water/kg-dry wood
W	width of cell, m
W_H	thickness of horizontal cell wall, m
W_V	thickness of vertical cell wall, m
x, y, z	coordinates, m
X, Y	dimensionless coordinates

Greek symbols

α	geometric function $= 1 + \beta^2$
β	geometric function $= \tan\theta$
η	transformed coordinate
Λ	dimensionless thermal conductivity $= \lambda/\lambda_{air}$
λ	thermal conductivity W/m K
$\lambda_x^*, \lambda_y^*, \lambda_z^*$	measured values by thermal conductivity meter
θ	inclination angle of cell wall, degree
Θ	dimensionless temperature $= (T - T_b)/(T_{t'} - T_b)$
ξ	transformed coordinate
ρ	density, kg/m^3

Subscripts

0	uncompressed wood
air	air
b	bottom plane
e	east plane
i	value at $t = 0$
t	top plane
w	west plane
wall	cell wall

2. Compressed woods

2.1. Producing process

The producing process for the compressed wood for $C_r = 1/2$ is schematically depicted in Fig. 1. This producing process is called as the high-temperature and high-pressure steam method [2]. It consists of three main processes, namely:

1. the plasticizing process,
2. the compression process, and
3. the fixation process.

An uncompressed wood was set into the forming die in the pressure vessel. Then, water was infused up to the bolster level. The water was heated by electric heaters up to 180 °C. The temperature rising speed was about 1.5 to 2 °C/min. The pressure in the vessel reached 0.98 MPa. The pressure vessel above water was filled with the saturated vapor. This heating process is the plasticizing process. This process is very important to avoid the destruction of the cell walls of the wood during the compression process. Then, the wood began to be compressed by the side moving-ram with the punch. The compression direction is the radial direction and the compression was conducted at the constant compression speed of 5 mm/min. After the compression process, it turned to the shape fixation process. The most reliable high-temperature and high-pressure steam method was

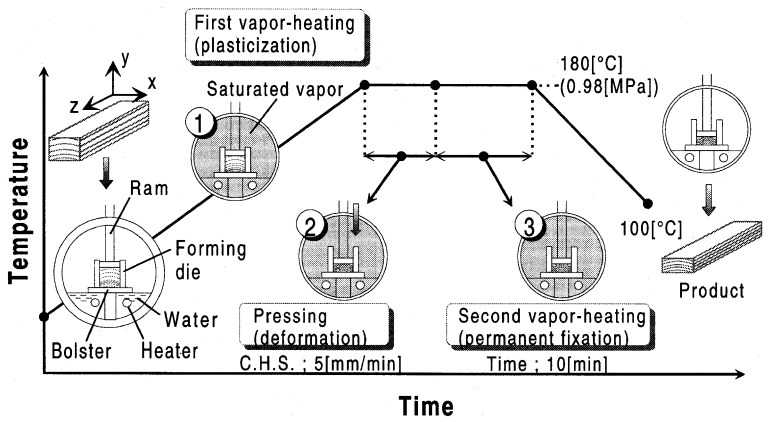

Fig. 1. A schematic diagram of producing process.

Table 1
Property of test pieces

Test piece (Japanese cedar)		Moisture content u (%)	Density ρ (kg/m^3)
#1	$C_r = 1$ (sapwood)	17.5	331
#2	$C_r = 1$ (heartwood)	7.15	351
#3	$C_r = 1$ (heartwood)	24.2	407
#4	$C_r = 4/5$ (sapwood)	21.3	377
#5	$C_r = 3/5$ (sapwood)	15.5	558
#6	$C_r = 1/2$ (sapwood)	4.08	741
#7	$C_r = 1/2$ (heartwood)	4.82	932
#8	$C_r = 1/3$ (sapwood)	5.51	960

adopted for the shape fixation. Namely, the shape was fixed by the secondary heating process in the pressure vessel of 180 °C and 0.98 MPa for 10 min.

The classical boiling method was adopted for the plasticizing process of the test pieces of $C_r = 4/5$, 3/5 and 1/3. The boiling time was 60 min. The selected compression speed was 15 mm/min. The drying set of 180 °C for 60 min was adopted for the shape fixation process.

2.2. Moisture content and density

In the present study, the effective thermal conductivities of the compressed Japanese cedars of the compression ratio $C_r = 4/5$, 3/5, 1/2 and 1/3 were measured. The measurements for both the heartwood and the sapwood were conducted for the test pieces of $C_r = 1$ and 1/2. And the measurements for the uncompressed woods were also conducted.

It is well known that the effective thermal conductivity of a wood is affected by the moisture content of the wood (e.g. [3]). Then, the moisture content of the specimens was measured by using a thermo-gravimetry and differential thermal analyzer (Shimadzu Seisakusyo, DTG-60). The moisture content u and density ρ of the specimens are tabulated in Table 1.

3. Measurement of effective thermal conductivity

3.1. Evaluation method of thermal conductivity of non-isotropic material

The effective thermal conductivities of the compressed Japanese cedars were measured by using a thermal conductivity meter (Kyoto electronics industry, TCR-01) that was based on the unsteady hot-wire method. The hot-wire of the probe is made of a constantan wire of 0.3 mm diameter, and type K thermocouple of 0.3 mm diameter is welded on its surface. It is well known that a wood is a non-isotropic medium, since the thermal conductivity in the fiber direction is 2 or 3 times higher than those tangential and radial directions. The unsteady hot-wire method is usually used for the measurement of an isotropic medium, however, it can be used for the measurement of a non-isotropic medium whose principal directions of heat conduction are known [4].

Here, we define the tangential direction, the radial direction and the fiber direction of a wood as x, y and z, respectively. The y is also the compression direction. These directions can be considered as principal directions of heat conduction. As shown in Figs. 2(a)–(c), the hot-wire probe (thick solid line in the figures) was put parallel to each x, y and z direction, and the measurements were conducted. However, these measured values are not the true thermal conductivities. The measured values by the thermal conductivity meter are denoted by λ_x^*, λ_y^* and λ_z^*, respectively. Takegoshi et al. [4] analytically obtained the following correlations between true thermal conductivity λ_x, λ_y and λ_z and measured values λ_x^*, λ_y^* and λ_z^* for the case where the principal directions coincide with the hot-wire directions.

$$\lambda_x = \frac{\lambda_y^* \lambda_z^*}{\lambda_x^*}, \quad \lambda_y = \frac{\lambda_z^* \lambda_x^*}{\lambda_y^*}, \quad \lambda_z = \frac{\lambda_x^* \lambda_y^*}{\lambda_z^*}. \tag{1}$$

3.2. Validity of Eq. (1)

Takegoshi et al. [4] made the comparison with the evaluated values from Eq. (1) and values measured by a one-dimensional steady method for few materials. Both values agree well within several percent in error. However, the measured values include the experimental uncertainty. Then, the validity of Eq. (1) is numerically confirmed for a case $\lambda_x = \lambda_y \neq \lambda_z$. In such a case, $\lambda_x^* = \lambda_y^*$. Then Eq. (1) can be written as

$$\lambda_x = \lambda_z^*, \quad \lambda_y = \lambda_z^*, \quad \lambda_z = \frac{\lambda_y^* \lambda_y^*}{\lambda_z^*} \left(= \frac{\lambda_x^* \lambda_x^*}{\lambda_z^*} \right). \tag{2}$$

The model to confirm the validity of Eq. (1) is schematically depicted in Fig. 3. Two-dimensional non-isotropic medium whose thermal conductivities in x and z directions are λ_x and λ_z, respectively, is considered. This simulates the situation that the hot-wire lies in the y direction. The cross-section of the medium is a square

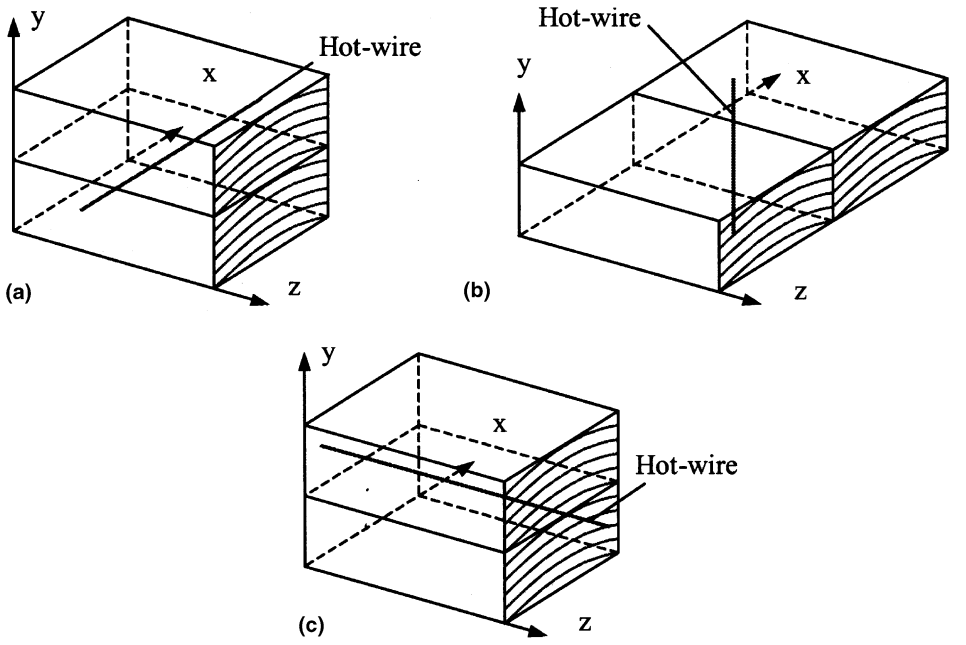

Fig. 2. A schematic diagram of measurement in three directions: (a) tangential (x) direction; (b) radial (y) direction; (c) fiber (z) direction.

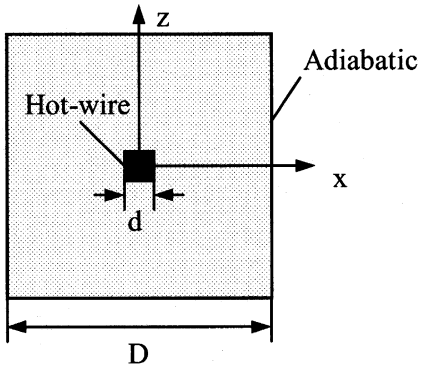

Fig. 3. A schematic diagram of numerical model.

whose side length is D. And the hot-wire represents a square rod of d. The constant electric power $\dot{q}_{\text{wire}}$ (W/m) is supplied to the hot-wire per unit length at time $t = 0$. The unsteady heat conduction equation can be expressed as:

$$\rho c \frac{\partial T}{\partial t} = \frac{\partial}{\partial x}\left(\lambda_x \frac{\partial T}{\partial x}\right) + \frac{\partial}{\partial z}\left(\lambda_z \frac{\partial T}{\partial z}\right) + \frac{\dot{q}_{\text{wire}}}{d^2}, \tag{3}$$

where ρ and c are the density and the specific heat of the medium, respectively. The medium is large enough, so that the temperature at the outer boundary does not change even though the outer boundary is adiabatic. The medium is initially kept at temperature T_i. The initial condition and the boundary condition are

$$\begin{aligned} t < 0: \quad & T = T_i, \\ t > 0, \quad & \text{on outer boundary} : \frac{\partial T}{\partial x} = \frac{\partial T}{\partial z} = 0, \\ & \text{in hot-wire region} : \lambda_x = \lambda_z = \infty, \\ & \text{in medium region} : \dot{q}_{\text{wire}} = 0. \end{aligned} \tag{4}$$

The numerical computations were carried out to solve Eq. (3). The numerical methodology used was the control volume method of Patankar [5]. The temperatures on the surface of the hot-wire at $t = t_1$ and t_2 are denoted by T_1 and T_2, respectively. Then,

$$\lambda_y^* = \frac{\dot{q}_{\text{wire}}}{4\pi} \frac{\ln(t_2/t_1)}{T_2 - T_1}. \tag{5}$$

Substituting λ_y^* into Eq. (2), then λ_z is obtained, since λ_z^* is identical with λ_x. The computations were conducted for the cases for $\lambda_x = 0.1$–0.4 W/m K, $\lambda_z = 0.2$–0.8 W/m K and $D = 0.1$ m, $d = 4 \times 10^{-4}$ m and for $t_1 = 60$ s and $t_2 = 600$ s. The deviation between true and evaluated values is plotted in Fig. 4. The maximum deviation in this computational range is about 1.4%.

3.3. Measurement procedure

In the unsteady hot-wire method, the hot-wire is heated by electric current. The temperature on the hot-wire rises rapidly and this temperature rise is propagating outward in a specimen. A specimen should be large enough so that the temperature on the outer surface of the specimen keeps constant during the

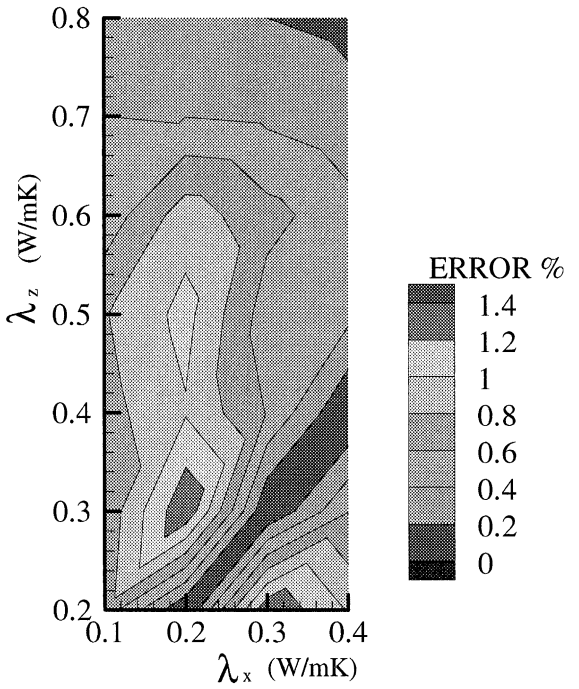

Fig. 4. Deviation between true and evaluated values.

measurement. In the present study, the size of the specimen and the electric current were determined by numerical simulations. The sizes of the specimen and the electric current chosen are listed in Table 2. In the unsteady hot-wire method, the temperature of the specimen must be uniform at the beginning of the measurement, therefore, it took sufficient time interval between measurements when the measurements were repeated.

4. Effective thermal conductivity

The thermal conductivities of the compressed Japanese cedars are plotted in Figs. 5–7. Figs. 5–7, respectively, represent the effective thermal conductivity in the tangential (x), radial (y) and fiber (z) directions. The

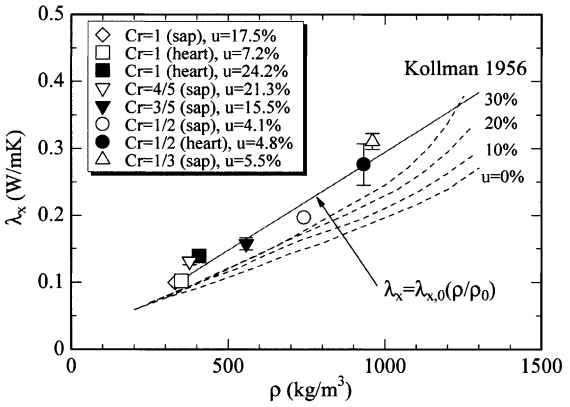

Fig. 5. Thermal conductivity in tangential (x) direction.

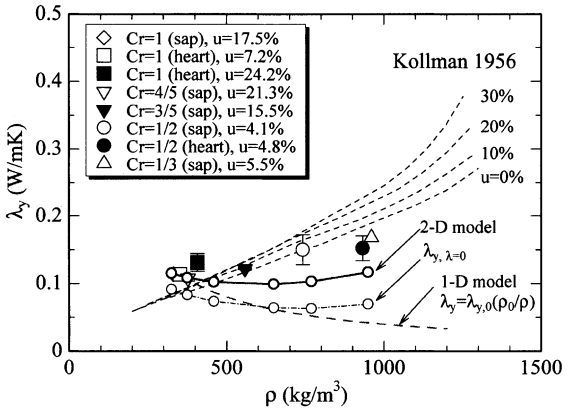

Fig. 6. Thermal conductivity in radial (y) direction.

dashed lines in Figs. 5 and 6 represent the effective thermal conductivity normal to the fiber direction of an uncompressed wood with a moisture content of 0–30%, $\lambda_{\perp}$ (e.g. [6]). The dashed line in Fig. 7 represents the thermal conductivity in the fiber direction of an uncompressed wood with a moisture content of 0% $\lambda_{//}$ (e.g. [7]). The measured conductivities of the uncompressed wood in both directions are slightly higher than the literature data.

Table 2
Measurement conditions

Test piece		Size (mm^3)	Time (s)	Current (A)
#1	$C_r = 1$ (sapwood)	$100 \times 100 \times 50$	600	0.6
#2	$C_r = 1$ (heartwood)	$100 \times 100 \times 50$	600	0.6
#3	$C_r = 1$ (heartwood)	$100 \times 100 \times 50$	600	0.6
#4	$C_r = 4/5$ (sapwood)	$100 \times 35 \times 20$	300	0.3
#5	$C_r = 3/5$ (sapwood)	$100 \times 35 \times 20$	300	0.3
#6	$C_r = 1/2$ (sapwood)	$120 \times 68 \times 35$	600	0.6
#7	$C_r = 1/2$ (sapwood)	$120 \times 68 \times 35$	600	0.6
#8	$C_r = 1/3$ (sapwood)	$100 \times 35 \times 20$	300	0.3

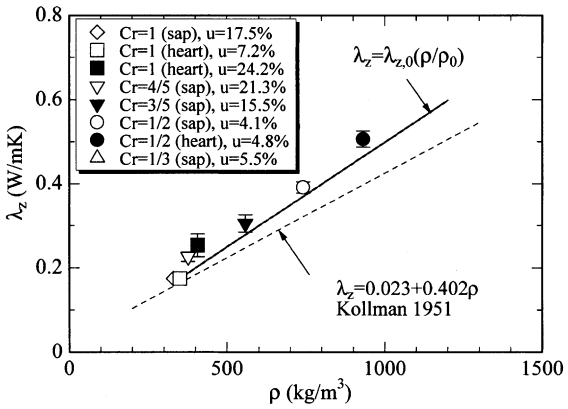

Fig. 7. Thermal conductivity in fiber (z) direction.

As shown in the figure, the effective thermal conductivities in the tangential direction, λ_x, and the fiber direction, λ_z, of the compressed woods increase proportionally to the density increment due to the compression. However, the effective thermal conductivity in the compression (radial) direction, λ_y, increases slightly with the density increment. The effective thermal conductivity of the compressed wood is lower than that of the uncompressed wood in the range of $\rho > 800$ kg/m^3. This thermal characteristic is desirable for the compressed wood.

Photographs of cell walls of the uncompressed wood (#1) and the compressed wood (#6) observed by a laser-microscope are shown in Figs. 8(a) and (b), respectively. The cell walls of the compressed wood are bent by compression. The schematic diagrams of the cell wall of

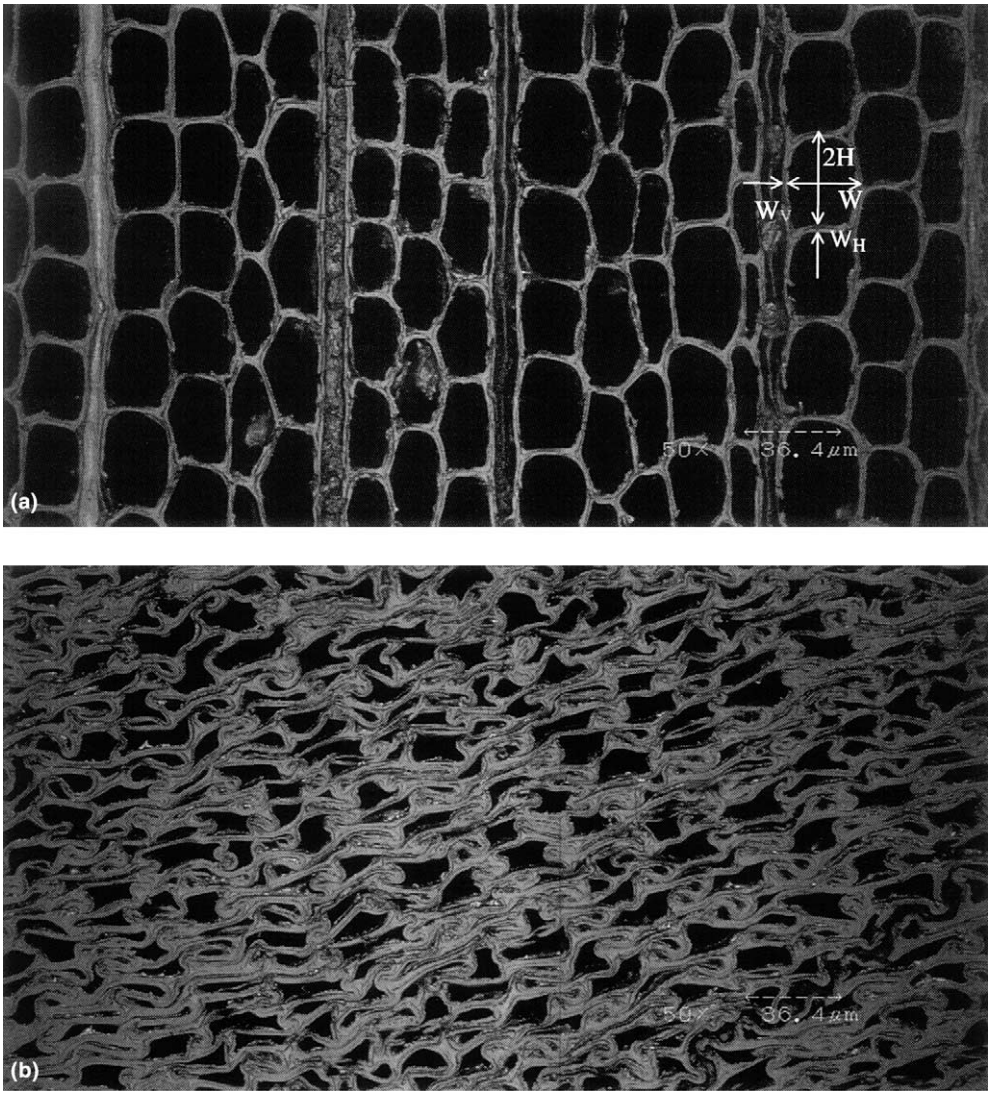

Fig. 8. Photographs of cell walls (×50): (a) uncompressed wood; (b) compressed wood.

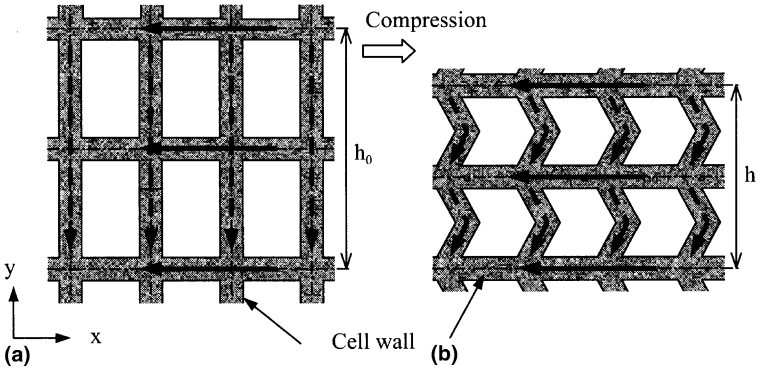

Fig. 9. One-dimensional heat conduction model: (a) uncompressed wood; (b) compressed wood.

the uncompressed and compressed woods are depicted in Figs. 9(a) and (b), respectively. The number of cell walls per unit area normal to the tangential (x) direction increases by compression. Since the thermal conductivity of the cell wall is higher than that of air, if the temperature gradient in the tangential (x) direction exists and one-dimensional heat conduction in the cell wall is considered, heat flux increases with increasing the number of horizontal cell walls. The solid arrows in the figure represent the heat flows. From this one-dimensional model, it can be explained that the effective thermal conductivity in the tangential (x) direction increases proportionally to the density increment due to the compression. This is also true in the fiber (z) direction.

In the case where the temperature gradient in the compression (y) direction exists, the situation is slightly complex. The dashed arrows in the figure represent the heat flows. The heat conducts in the bent walls as shown in Fig. 9(b). Here, the thicknesses of the wood before and after compressions are defined as h_0 and h, respectively. In this case, the heat conducting pass lengths before and after compressions are identical. Therefore, if the temperature differences between the top and bottom surfaces before and after compressions are identical, the heat fluxes are identical.

Here, the effective thermal conductivities before and after compressions are defined as λ_0 and λ, respectively. Then, the following equation is obtained:

$$\dot{q} = \lambda_0 \frac{\Delta T}{h_0} = \lambda \frac{\Delta T}{h}. \tag{6}$$

This can be rewritten as

$$\lambda = \lambda_0 (h/h_0) = \lambda_0 (\rho_0/\rho). \tag{7}$$

In the ideal situation, the effective thermal conductivity in the compression (y) direction decreases with the density increment due to the compression. This correlation is plotted in Fig. 6.

5. Formulation

5.1. Description of two-dimensional model

The characteristics of the thermal conductivities in the tangential and fiber directions are successfully explained by the one-dimensional model. But, the one-dimensional model fails to explain the characteristics of the thermal conductivity in the radial direction. Then, a two-dimensional model, in which two-dimensional heat conduction in the cell walls and the cavity is considered, is schematically depicted in Fig. 10. The following assumptions are made:

1. The cell geometry is rectangular.
2. The cell wall thickness is uniform but the thicknesses of the horizontal and vertical cell walls are different.
3. The cells of the same geometry are stacked in y (radial) direction and are aligned in x (tangential) direction.
4. Overall temperature gradient exists in y (radial) direction.
5. The temperature on the bottom plane is uniform.
6. The temperature on the top plane is also uniform.
7. The temperature field repeats itself in successive cells in x (tangential) direction.

Under these assumptions and the symmetric condition, it is possible to solve the heat conduction in only a half of a cell with periodic thermal boundary conditions. This half cell is surrounded by dashed line in the figure.

The detail of the half cell is shown in Fig. 11. Two-dimensional steady heat conduction equation can be expressed as:

$$\frac{\partial}{\partial x}\left(\lambda \frac{\partial T}{\partial x}\right) + \frac{\partial}{\partial y}\left(\lambda \frac{\partial T}{\partial y}\right) = 0. \tag{8}$$

The boundary conditions on the top and bottom boundaries are:

$$\begin{aligned} &\text{On top boundary :} \quad T = T_{\mathrm{t}}, \\ &\text{On bottom boundary :} \quad T = T_{\mathrm{b}}. \end{aligned} \tag{9}$$

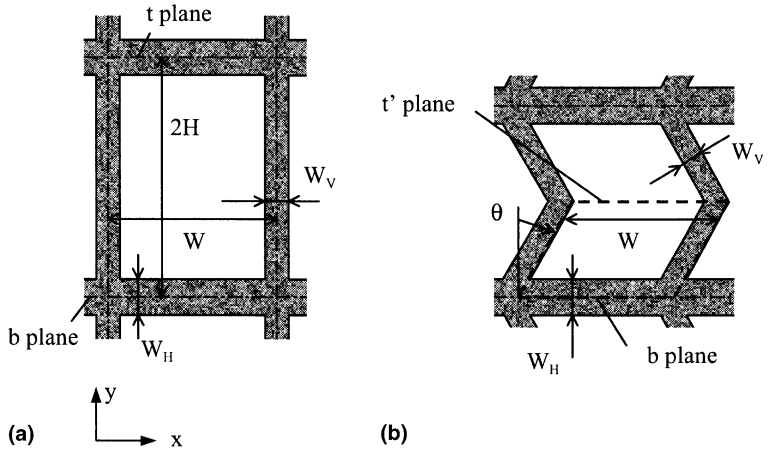

Fig. 10. Two-dimensional heat conduction model: (a) uncompressed wood; (b) compressed wood.

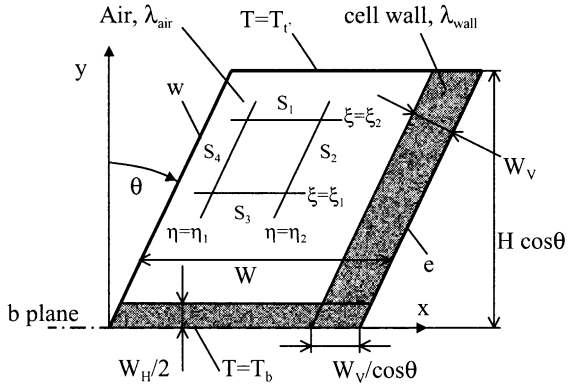

Fig. 11. Detail of a half cell and lines of constant η and ξ in the physical domain.

Both the side boundaries are the periodic boundary and are expressed as:

On east and west boundaries :

$$T_e = T_w, \quad \left(\frac{\partial T}{\partial x}\right)_e = \left(\frac{\partial T}{\partial x}\right)_w. \tag{10}$$

The following dimensionless variables are used:

$$X = \frac{x}{W}, \quad Y = \frac{y}{W}, \quad \Theta = \frac{T - T_b}{T_{t'} - T_b}, \quad \Lambda = \frac{\lambda}{\lambda_{air}}, \tag{11}$$

where W is the width of the cell and this is chosen for the reference length. Then upon introduction of the dimensionless variables and parameters, the governing equation has the following form:

$$\frac{\partial}{\partial X}\left(\Lambda \frac{\partial \Theta}{\partial X}\right) + \frac{\partial}{\partial Y}\left(\Lambda \frac{\partial \Theta}{\partial Y}\right) = 0. \tag{12}$$

5.2. Coordinate transformation

A simple algebraic coordinate transformation is used that maps the parallelogram cross-section onto a rectangle. Specifically, the X and Y coordinates are transformed into η and ξ coordinates by the relations

$$\eta = X - Y\tan\theta, \quad \xi = Y. \tag{13}$$

In terms of the new coordinates, the solution domain is bounded by $0 < \eta < 1$, $0 < \xi < (H/W)\cos\theta$. The transformed equation and their discretization and solutions are documented in a paper by Asako and Faghri [8]. A simple description will be given here. Lines of constant η and ξ are illustrated in Fig. 11. A control volume which is used for the discretization contains between $\eta = \eta_1$ and $\eta = \eta_2$, and $\xi = \xi_1$, $\xi = \xi_2$.

Integrating the heat conduction equation over a control volume in physical space bounded by lines constant η and ξ, Eq. (12) becomes

$$\int_S \left(\Lambda \vec{n} \cdot \vec{\nabla}\Theta\right) \mathrm{d}S = 0. \tag{14}$$

For evaluation of the surface integrals, expressions are needed for the element of surface $\mathrm{d}S$, the gradient operator $\vec{\nabla}$, and unit vector $\vec{n}$. The surface integral is subdivided into a sum of four surface integrals, respectively, over the segments S_1, S_2, S_3, and S_4.

$$\text{For surface } S_1: \quad \vec{n} = \vec{e}_Y, \quad \mathrm{d}S = \mathrm{d}\eta, \tag{15}$$

$$\text{For surface } S_2: \quad \vec{n} = (\vec{e}_X - \beta\vec{e}_Y)\alpha^{-1/2}, \quad \mathrm{d}S = \alpha^{1/2}\,\mathrm{d}\xi, \tag{16}$$

where

$$\beta = \tan\theta, \quad \alpha = 1 + \beta^2 = 1/\cos^2\theta \tag{17}$$

and

$$\vec{\nabla} = \left(\frac{\partial}{\partial\eta}\right)_{\xi}\vec{e}_X + \left\{\left(\frac{\partial}{\partial\xi}\right)_{\eta} - \beta\left(\frac{\partial}{\partial\eta}\right)_{\xi}\right\}\vec{e}_Y. \tag{18}$$

For surfaces S_3 and S_4, dS is identical to those for S_1 and S_2, with the exception that the outward normal $\vec{n}$ has the opposite sign.

Using Eqs. (16)–(18), Eq. (14) can be rewritten as

$$\int_{S_1} \Lambda\left(\frac{\partial\Theta}{\partial\xi} - \beta\frac{\partial\Theta}{\partial\eta}\right)\mathrm{d}\eta - \int_{S_3} \Lambda\left(\frac{\partial\Theta}{\partial\xi} - \beta\frac{\partial\Theta}{\partial\eta}\right)\mathrm{d}\eta + \int_{S_2} \Lambda\left(\alpha\frac{\partial\Theta}{\partial\eta} - \beta\frac{\partial\Theta}{\partial\xi}\right)\mathrm{d}\xi - \int_{S_4} \Lambda\left(\alpha\frac{\partial\Theta}{\partial\eta} - \beta\frac{\partial\Theta}{\partial\xi}\right)\mathrm{d}\xi = 0. \tag{19}$$

The control volume formulation of the problem is completed. Derivatives in η and ξ directions in Eq. (19) can be easily discretized and a set of algebraic equations can be obtained.

5.3. Heat flux and effective thermal conductivity

The heat flux normal to the bottom plane (-y direction) can be expressed as:

$$\dot{q} = -\vec{e}_y \cdot \vec{q} = \frac{\lambda_{\mathrm{wall}}(T_{t'} - T_{\mathrm{b}})}{W}\left(\frac{\partial\Theta}{\partial\xi} - \beta\frac{\partial\Theta}{\partial\eta}\right)_{\mathrm{b}}. \tag{20}$$

On the bottom plane, $\Theta = 0$, therefore $\partial\Theta/\partial\eta = 0$. Then, Eq. (20) becomes

$$\dot{q} = \frac{\lambda_{\mathrm{wall}}(T_{t'} - T_{\mathrm{b}})}{W}\left(\frac{\partial\Theta}{\partial\xi}\right)_{\mathrm{b}}. \tag{21}$$

The total heat conduction rate $\dot{Q}$ from the bottom plane with $\mathrm{d}s = w\,\mathrm{d}\eta$ is

$$\dot{Q} = \int_0^w \dot{q}\,\mathrm{d}s = \lambda_{\mathrm{wall}}(T_{t'} - T_{\mathrm{b}})\int_0^1 \left(\frac{\partial\Theta}{\partial\xi}\right)_{\mathrm{b}}\mathrm{d}\eta. \tag{22}$$

The heat conduction rate in a plate whose effective thermal conductivity in the y (radial) direction is λ_y, temperature difference is $T_{t'} - T_{\mathrm{b}}$, and the thickness is $H\cos\theta$ can be expressed as:

$$\dot{Q} = \lambda_y \frac{T_{t'} - T_{\mathrm{b}}}{H\cos\theta}W. \tag{23}$$

Then, the effective thermal conductivity λ_y of the compressed wood can be expressed as:

$$\frac{\lambda_y}{\lambda_{\mathrm{air}}} = \left(\frac{\lambda_{\mathrm{wall}}}{\lambda_{\mathrm{air}}}\right)\left(\frac{H}{W}\right)\cos\theta\int_0^1 \left(\frac{\partial\Theta}{\partial\xi}\right)_{\mathrm{b}}\mathrm{d}\eta. \tag{24}$$

Solving the set of algebraic equations, the temperature is obtained. A line-by-line method is used to solve the algebraic equations. From the temperature of the cell, heat flux by conduction can be evaluated. The discretized procedure of the integral form of the conduction equation is similar to the work documented by Asako and Faghri [8] and will not be discussed here. All computations were performed with (52×82) grid points. These grid points are distributed in a non-uniform manner with a higher concentration of grids close to the interfaces of the cell wall and cavity as shown in Fig. 13 with the isotherms. 20 grid points are assigned in each cell wall. Supplementary runs were performed with (26×42) and (38×58) grid points to investigate grid size effects for the inclination angle of $\theta = 45°$. The change in $\lambda_y/\lambda_{\mathrm{air}}$ between the coarse mesh (26×42) and the fine mesh (52×82) was 1.0%. And the change in $\lambda_y/\lambda_{\mathrm{air}}$ between the medium mesh (38×58) and the fine mesh (52×82) was only 0.3%.

6. Numerical results

The computational parameters which have to be specified prior to the computation are the thermal conductivity ratio, $\lambda_{\mathrm{wall}}/\lambda_{\mathrm{air}}$, the aspect ratio of the cell, H/W, dimensionless cell wall thicknesses W_{V}/W and W_{H}/W and the inclination angle θ. The reported values for the thermal conductivity of the cell wall, λ_{wall}, range from 0.36 [9] to 0.654 [10]. Here, $\lambda_{\mathrm{wall}} = 0.654$ reported by Maku [10] was used for computations. And the thermal conductivity for air at 20 °C, $\lambda_{\mathrm{air}} = 0.0256$ [3], was used.

As seen in Fig. 8, the width and height of the cell and also the cell wall thickness of each cell are not identical. Therefore, the width of the cell, W, the height, H, and the cell wall thicknesses, W_{V} and W_{H}, were measured for 56 uncompressed cells. Cells are not exact rectangles too. Therefore, W is measured at the mid-height of the cell as shown in the figure. And also H is measured at the mid of the cell. The cell wall thicknesses W_{H} and W_{V} are also measured at the mid of the cell. The W_{V}/W and W_{H}/W of all cells are plotted as a function of H/W in Fig 12. The ranges of W_{V}/W, W_{H}/W and H/W and its average values are tabulated in Table 3. The computations were conducted for the geometry of the average values and for $\theta = 0°$, 30°, 45°, 60°, 65° and 70°.

The density of the cell for $\theta = 0$ can be easily calculated from the geometrical shape as

$$\rho_0 = \left[\left(1 - \frac{W_{\mathrm{V}}}{W}\right)\left(\frac{H}{W} - 0.5\frac{W_{\mathrm{H}}}{W}\right)\rho_{\mathrm{air}} + \left\{0.5\frac{W_{\mathrm{H}}}{W}\left(1 - \frac{W_{\mathrm{V}}}{W}\right) + \frac{W_{\mathrm{V}}}{W}\frac{H}{W}\right\}\rho_{\mathrm{wall}}\right] \Big/ H/W. \tag{25}$$

The density of the cell wall and the density of the air at 20 °C are $\rho_{\mathrm{wall}} = 1560\ \mathrm{kg/m^3}$ [9] and $\rho_{\mathrm{air}} = 1.161\ \mathrm{kg/m^3}$ [3], respectively. The calculated density of the cell of the average geometry for $\theta = 0$ is $\rho_0 = 324.6\ \mathrm{kg/m^3}$. The density of the compressed cell can be calculated by

$$\rho = \frac{\rho_0}{\cos\theta}. \tag{26}$$

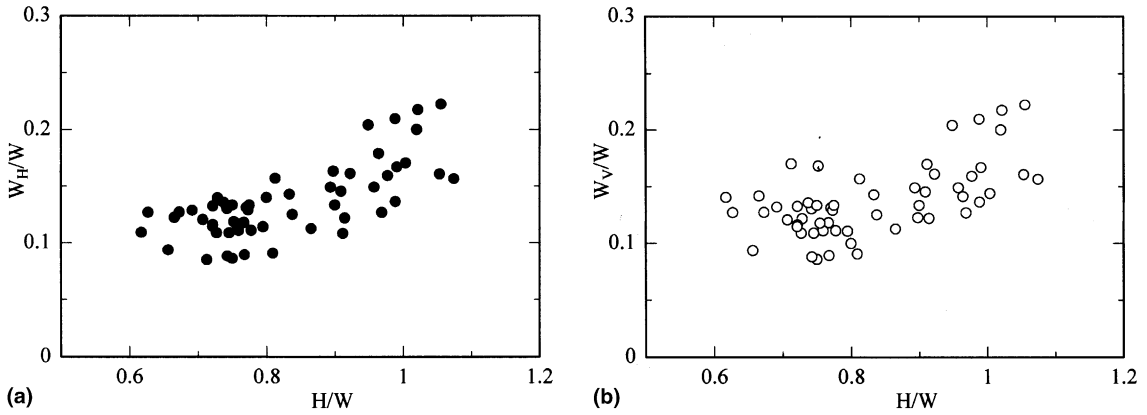

Fig. 12. Cell geometry: (a) W_H/W vs H/W; (b) W_V/W vs H/W.

Table 3
Dimensionless cell geometry

	H/W	W_V/W	W_H/W
Maximum	0.61	0.088	0.086
Minimum	1.07	0.22	0.24
Average	0.829	0.137	0.136

The correlation between the compression ratio, C_r, and the inclination angle, θ, can be expressed from the identity of the compression ratio as

$$C_r = \frac{\rho_0}{\rho} = \cos\theta. \tag{27}$$

Therefore, $\theta = 0°$, 30°, 45°, 60°, 65° and 70° correspond to $C_r = 1$, 0.866, 0.707, 0.5, 0.423 and 0.342, respectively.

The computed effective thermal conductivity in the radial direction is plotted in Fig. 6 as a function of the density. The solid line represents the results of the present computations. The chain line in the figure represents the result by the one-dimensional heat conduction analysis in which heat conduction in the cavity was neglected. The discrepancy between the measured values and the results by the simple one-dimensional analysis was extremely large. However, discrepancy between the measured values and the present numerical results is small. The fact that the measured effective thermal conductivity increases slightly with the density increment can be explained by considering both heat conduction in cell walls and cavity.

The contour plot of the temperature for $\theta = 60°$ ($C_r = 1/2$) is presented in Fig. 13. The interval of the isotherms is equal of $\Delta\Theta = 0.1$. It is well known that the heat travels normal to the isotherm. As seen from the figure, the isotherm and the cell wall intersect with an inclination angle. This indicates that there exists the heat flow from air to the cell wall across the cell cavity. Although the thermal conductivity of the air is low, the air in the cavity may affect the heat conduction in the cell. Supplementary runs were performed to confirm the effect of air on the heat conduction rate. Namely, the

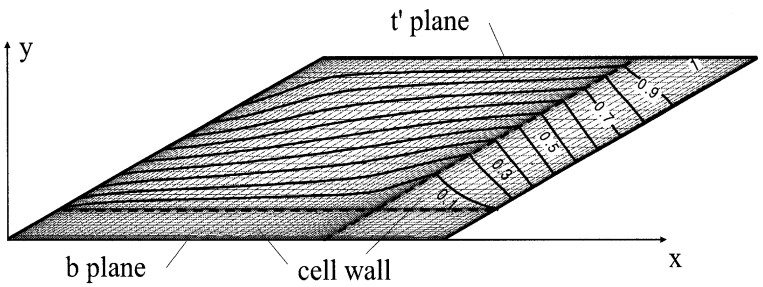

Fig. 13. Contour plot of isotherm for $\theta = 60°$.

Table 4
Contribution of air to effective thermal conductivity

θ	$(\lambda_y - \lambda_{y,\lambda=0})/\lambda_y \times 100\%$
0	20.8
30	23.8
45	28.3
60	35.7
65	38.7
70	40.7

computations were performed with an assumption of $\lambda = 0$ for air in the cavity and the effective thermal conductivities for such a situation, $\lambda_{y,\lambda=0}$, were obtained. The comparison with the ordinary effective thermal conductivity was made and the results are tabulated in Table 4. The contribution of the air to the effective thermal conductivity, $(\lambda_y - \lambda_{y,\lambda=0})/\lambda_y$, in the case of the uncompressed wood ($\theta = 0$) is 20.8%. This rate increases with the density increment. It is noteworthy that the rate reaches 40.7% in the case of $\theta = 70°$ ($C_r = 0.342$). The effective thermal conductivity, $\lambda_{y,\lambda=0}$, is also plotted by a chain line in Fig. 6.

7. Concluding remarks

The effective thermal conductivities of compressed Japanese cedars (*cryptomeria japonica*) were measured by using the unsteady hot-wire method. Numerical computations were performed to explain the characteristics of the effective thermal conductivity in the radial direction by using a microscopic two-dimensional heat conduction model for the compressed wood. The following conclusions are obtained:

1. The effective thermal conductivities in the fiber direction, λ_z, and the tangential direction, λ_x, increase proportionally to the density increment due to the compression.
2. The effective thermal conductivity in the radial (compressed) direction, λ_y, slightly increases with the density increment. This thermal characteristic is desirable when the compressed wood is applied for the window frames.
3. The fact that the measured effective thermal conductivity in radial direction increases slightly with the density increment can be explained by considering both heat conduction in cell walls and cavity. The effect of air in the cavity on the effective thermal conductivity increases with the density increment.

Acknowledgements

This research was partly supported by a Grant-in-Aid for Scientific Research (10555250) sponsored by the Ministry of Educatioin, Science, Sports and Culture, Japan. And also the Fig. 8 was taken by a laser-microscope of Lasertech Corp. (1HD200). The authors thank for their courtesy.

References

[1] H. Nishimura, Processing technology for value addition to wood, J. JSTP 41 (478) (2000) 1087–1092.
[2] T. Hata, Vapor-jetting compression method, Wood Industry 49 (1) (1994) 2–7.
[3] Japan Society of Thermophysical Properties, Thermophysical Properties Handbook, Yokendo, Tokyo, 1990, p. 210.
[4] E. Takegoshi et al., A method of measuring the thermal conductivity of orthogonal anisotropic materials by transient hot wire method, Trans. JSME, Ser. B 48 (433) (1982) 1743–1750.
[5] S.V. Patankar, in: Computation of Conduction and Duct Flow Heat Transfer, Innovative Research, Minneapolis, 1991, pp. 14–16.
[6] F. Kollman, L. Malmquist, Über die Wärmeleitzahl von Holz u. Holzwerkstoffen, Holz Roh-Werkstoff 14 (6) (1956) 201–208.
[7] F. Kollman, in: Technologie des Holzes und der Holzwerkstoffe I, Springer, Berlin, 1951, p. 506.
[8] Y. Asako, M. Faghri, Finite-volume solutions for laminar flow and heat transfer in a corrugated duct, J. Heat Transfer 109 (1987) 627–634.
[9] T. Harada et al., Thermal constants of wood during the heating process measured with the laser flash method, J. Wood Sci. 44 (1998) 425–431.
[10] T. Maku, Studies on the heat conduction in wood, Wood Res. 13 (1954) 1–80.